Determination of conventional velocity gradient (G) using CFD technique for a pilot-scale flocculation system

Yamuna S. Vadasarukkai and Graham A. Gagnon

ABSTRACT

Achieving uniform mixing conditions are essential for the flocculation process to optimize floc size and avoid floc-breakup. Limited literature is available on establishing consistent operational conditions and procedures for pilot-scale flocculation systems, which have tank sizes smaller than full-scale and larger than jar-test equipment. In this study, the influence of mixing speeds on the determination of the conventional design parameter, the average velocity gradient (*G*), was investigated for pilot-scale paddle flocculators. The pilot-scale plant for this paper was hosted at the J.D. Kline Water Supply Plant (JDKWSP) in Halifax, Canada. Computational fluid dynamics (CFD) was evaluated as an alternative design technique and compared against traditionally used empirical-based calculations. Comparison of both approaches showed that the *G*-values of empirical method were substantially higher than the predicted values for rotational speeds greater than 5 rpm. In contrast, CFD predictions found that *G*-values used for tapered paddle flocculation process (up to 60 s^{-1}) could be achieved at lower rotational speed (around 15 rpm), which minimizes the power input required for mixing. The practical implications of operating at higher than required *G*-values relates to potential negative consequences such as floc break up, and the reliance of chemical additives to avoid floc break-up. These very practical outcomes could impact the interpretation of findings from pilot-scale treatment systems.

Key words | average velocity gradient (*G*), computational fluid dynamics, flocculation, hydrodynamics, pilot-scale water treatment

Yamuna S. Vadasarukkai
Graham A. Gagnon (corresponding author)
Department of Civil & Resource Engineering,
Dalhousie University,
Halifax NS B3J 1Z1,
Canada
Tel.: 902.494.3268
Fax: 902.494.3108
E-mail: *graham.gagnon@dal.ca*

NOMENCLATURE

A_P	projected area of paddle (m^2)
C	mean tracer concentration ($kg\,m^{-3}$)
C_D	drag coefficient on paddle for turbulent flow (dimensionless number)
CFD	computational fluid dynamics
FE	finite element
FTC	flow through curve
FV	finite volume
F_D	drag force on paddles
G	global root mean square velocity gradient or energy input rate (s^{-1})
HRT	hydraulic retention time
JDKWSP	J.D. Kline Water Supply Plant
MRF	multiple reference frame
N	shaft rotational speed (rpm)
NaOH	sodium hydroxide
NOM	natural organic matter
P	power of mixing input to entire mixing vessel ($J\,s^{-1}$)
Re	Reynolds number for paddle flocculators (dimensionless number)
RTD	residence time distribution
t	time (s)

doi: 10.2166/aqua.2010.081

V	volume of mixing vessel (m^3)
QUICK	quadratic upstream interpolation for convective kinetics
r_1, r_2, r_3	distance from the center of rotation to the centerline of inner, middle and the outer paddles respectively (m)
3D	three-dimensional

Greek letters

C_μ	modelling constant = 0.09
ρ	fluid density ($kg\,m^{-3}$)
x_i	Cartesian co-ordinates components (m)
u_i	Cartesian velocity components relative to the rotating frame of reference ($m\,s^{-1}$)
p	pressure (Pa)
ε_{ijk}	unit alternating tensor
Ω_i	component of rotational speed of the reference frame ($rad\,s^{-1}$)
τ_{ij}	shear stress tensor ($N\,m^{-2}$)
δ_{ij}	Kronecker delta
μ_t	turbulent viscosity ($kg\,m^{-1}s^{-1}$)
k	turbulent kinetic energy ($m^2\,s^{-2}$)
ε	turbulent kinetic energy dissipation per unit mass for vessel ($m^2\,s^{-3}$)
σ_c	turbulent Schmidt number for the tracer = 1.0
μ	dynamic viscosity of water ($kg\,m^{-1}s^{-1}$)
ν	kinematic viscosity of water ($m^2\,s^{-1}$)

INTRODUCTION

Flocculation processes are designed to promote the agglomeration of destabilized particles that can be subsequently removed in clarification and/or filtration (Gao *et al.* 2002; Betancourt & Rose 2004). Destabilized particles are achieved through appropriate coagulant dosing and optimal pH conditions that are specific to the primary particles in the water matrix and the overall water quality characteristics (e.g. alkalinity, conductivity). The flow conditions in flocculation tanks are driven by localized turbulence whereby shear plays a dominant role in enhancing the rate of collision between coagulant, destabilized particles and primary particles present in water (Luo 1997; Haarhoff & Van der Walt 2001; Crittenden *et al.* 2005; Zhang 2006; Bridgeman *et al.* 2008).

Since its initial development (e.g. Black *et al.* 1957), the jar test has remained the conventional method of understanding coagulation chemistry and optimizing flocculation mixing. A noted criticism of this ubiquitous tool relates to the reactor similitude to the true hydraulic conditions of full-scale coagulation/flocculation processes (TeKippe & Ham 1970). Although the use of traditional jar tests for flocculation control provide some indication of the appropriate type and concentration of flocculants, Argaman (1971) argued that pilot-plant studies are essential for assuring the success of the design of new plants. More recently, pilot-scale studies have been key tools for optimizing the removal of microbial contaminants and natural organic matter (NOM) in treatment processes that utilize coagulation and flocculation (Nieminski & Ongerth 1995; Dugan *et al.* 2001; States *et al.* 2002; Betancourt & Rose 2004; Xagoraraki *et al.* 2004).

Pilot-scale studies of a continuous conventional treatment system (coagulation, flocculation, sedimentation and filtration) have been able to show that under the effectiveness of coagulation pretreatment, the treatment system could achieve more than 4-log total *Cryptosporidium* removal (Dugan *et al.* 2001). Several interrelated criteria govern the efficiency and effectiveness of the coagulation and flocculation stages; such as coagulant type and dosage, pH and mixing arrangement (Bridgeman *et al.* 2008). Extensive research has been conducted to understand the complex coagulation chemistry and to optimize the coagulant type and dosage in pilot-scale studies (Dugan *et al.* 2001; States *et al.* 2002). However, there is limited data available related to the optimization of the root mean square velocity gradient or *G*-value, the conventional design parameter developed by Camp & Stein (1943), and its associated impact in pilot-scale studies. In the pilot-scale study conducted by Dugan *et al.* (2001), the flocculation process took place in four stages with *G*-values of 30, 20, 15 and $10\,s^{-1}$ respectively. In contrast, the estimated G values were 70, 40 and $10\,s^{-1}$ for the three flocculation chambers of a pilot-scale treatment facility at the University of Wisconsin, Madison (Xagoraraki *et al.* 2004). Those studies relied on conventional design equations to determine *G*-values even though the flocculation geometry and flow conditions were unique to the pilot conditions.

As a result of difference in flocculation, impeller design and operating conditions (flow rate, temperature, rotational speed), it becomes necessary to investigate the hydrodynamics of the system for enhanced floc formation at optimal retention time. It is plausible that understanding these unique pilot designs would aid in scale-up to full-scale and to inter-pilot comparisons. In this study, the application of computational fluid dynamics (CFD) for evaluating the performance of paddle flocculators of the pilot-scale system of J.D. Kline Water Supply Plant (JDKWSP) in Halifax, Canada was examined. The main objective was to investigate the effect of rotational speeds of the paddle board on the flow-field characteristics and to establish an accurate methodology of calculating the *G*-values for the pilot-plant design.

METHODOLOGY

Description of pilot-scale system

The pilot-scale system commissioned by Halifax Water consists of two identical treatment trains to simulate the conventional treatment of JDKWSP. Each train comprises of three units of rapid mixing tanks, a three-stage flocculation chamber, a sedimentation basin and three dual media filtration units in parallel (Intuitech Inc., Salt Lake City, UT). Both the pilot trains were equipped with automated online monitoring and control equipment for measuring the key water quality parameters such as flow rate, temperature, rotational speed of mixers, pH, turbidity, and particle counting for the filters. Raw water from the full-scale system is pumped continuously at a constant flow rate of 15 L/min, measured using a calibrated inline flow meter. For this study, water leaving the flocculation processes bypassed sedimentation in both trains to replicate the direct filtration conditions occurring in the full-scale system.

The parallel trains consist of three stage flocculation to allow for tapered mixing. Vertical-shaft paddle flocculators were used to provide continuous mixing for suspension of the floc formed during flocculation in each stage (Figure 1). Each flocculation stage has a flow capacity of 189 L with theoretical hydraulic retention time (HRT) of 12.6 min (HRT = volume/flow rate). Based on empirical design

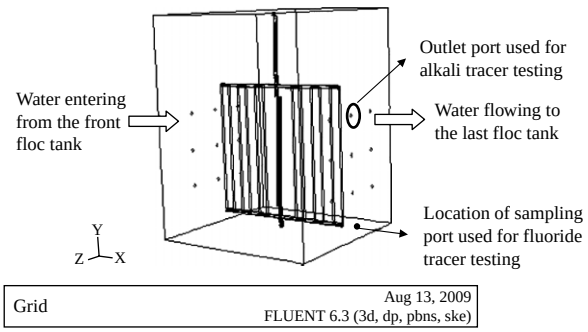

Figure 1 | A 3D geometry showing the inlet and outlet configuration of the middle floc tank of the three-stage paddle flocculation process of pilot-scale system at JDKWSP.

equations and specifications provided by the manufacturer tapered mixing was provided for each stage with *G*-values of $60\,s^{-1}$, $40\,s^{-1}$ and $20\,s^{-1}$. Using empirical Equations (6) and (7), the rotational speeds were calculated corresponding to the initial *G*-values and were set to rotate at 18.8, 14.3, and 9 rpm respectively. The inlet and outlet ports connecting the flocculation trains are of diameter 5.5 mm each. There are nine circular inlets and nine circular outlets in each floc train, arranged in 3 by 3 matrix format. The outlet for the final flocculation stage was designed with a single exit port (diameter 50.8 mm).

Residence time distribution (RTD) curve, also known as flow through curve (FTC), was determined for each flocculation stage through step input method. The FTC determined by step input method represents the cumulative distribution function of the detention times in the tank (Stamou 2008). These have the shape of an S-curve when plotted with respect to time, with a minimum of 0 and a maximum of 1 (Templeton *et al.* 2006). The FTC analysis investigates the effect of the rotational speed on the hydrodynamic flow characteristics (Ta 1999; Choi *et al.* 2004; Baawain *et al.* 2006; Svrcek *et al.* 2006; Templeton *et al.* 2006; Zhang 2006; Stamou 2008). Tracer testing is considered as a reliable approach for determining the hydraulic performance of a water treatment reactor (Svrcek *et al.* 2006). Both experimental and numerical (CFD) tracer studies were performed for the flocculation unit. The results from the tracer studies were used as a validation step for CFD predictions, which is consistent with studies reported by others (e.g. Essemiani & de Traversay 2002; Templeton *et al.* 2006; Zhang 2006).

CFD modelling procedure

CFD is the state of the art of predicting the hydrodynamics of fluid flow particularly and associated phenomena (e.g. contaminant mass transport), through the use of numerical modelling approach. In CFD, the Navier-Stokes equations coupled with the turbulence, species and/or multiphase transport equations governing the fluid flow are approximated to a system of algebraic equations using discretization techniques and are solved iteratively on a computer (Versteeg & Malalasekara 1995; Craig *et al.* 2002; Essemiani & de Traversay 2002; Zhang *et al.* 2008). Finite volume (FV) discretization method is the most well-established and thoroughly validated CFD technique used commonly in CFD software packages; for e.g. PHOENICS, ANSYS FLUENT, ANSYS CFX, FLOW3D, Flo++ and STAR-CD (Versteeg & Malalasekara 1995). In water and wastewater treatment processes, it has been widely used in investigation and optimization of plant design and operations (Haarhoff & Van der Walt 2001; Baawain *et al.* 2006; Templeton *et al.* 2006; Stamou 2008) and in flow distribution calculations in distribution channels (Ta 1999; Baek *et al.* 2005). Using CFX multiphase modelling approach, Zhang *et al.* (2008) could show for the first time that multiple sampling strategies are essential for improved ozone residual monitoring and tracer testing for full-scale ozone disinfection process. Bridgeman *et al.* (2008) combined both CFD modelling and experimental jar testing results to assess the floc strength and breakage for standard jar test apparatus.

Alternatively, other CFD software packages using finite element (FE) solvers such as COSMOL Multiphysics (formerly FEMLAB), FIDAP, Finlab are used to model complex flow patterns in treatment processes such as ultraviolet reactor (Downey *et al.* 1998), membrane processes (Subramani *et al.* 2006; Lerch 2008; Marcos *et al.* 2009) and ozone contactors (Wols *et al.* 2008). Ducoste & Clark (1999) used FIDAP to analyze the complex turbulence flow characteristics generated by rotating impellers in a square-stirred reactor. With the advancement in computing technology, the ability of CFD to model complex designs and flow processes through FV or FE numerical approaches has expanded its applicability in water and wastewater industries. Templeton *et al.* (2006) recommended that CFD can be accepted as a design and analytical tool by regulatory agencies, provided a detailed protocol for validating CFD is established. Although, CFD cannot replace the experimental analysis; it can be used as an additional tool to generate knowledge that can be integrated with the full-scale process design and operations by the utilities.

A three-dimensional (3D), single phase CFD modelling approach was carried out for the flocculation tank using commercially available software package, FLUENT 6.3.26 (ANSYS, Lebanon, NH). The Reynolds number (Re) for rotational speeds of 1 to 20 rpm ranged from 4,151 to 83,020. As mentioned in Shekhar & Jayanti (2002), the calculated *Re* was in the turbulence flow criterion ($Re > 480$) and hence, Standard $k-\varepsilon$ model was selected for modelling the turbulence flow. Multiple Reference Frame (MRF) model was as well incorporated to investigate the effect of rotational speeds on the *G*-value. In MRF modelling technique, two distinct frames of reference (or zones) were defined by creating a cylindrical interface with respect to the axis of rotation of the paddle shaft; thereby, dividing the geometry of flocculation tank into moving and stationary zones. The moving zone computes the flow occurring within the cylindrical interface that includes the paddle, shaft and the fluid flow surrounding it; while the stationary zone performs computation for the flow outside the interface. Additional terms such as Coriolis acceleration and centrifugal force acting on the fluid (water) due to the influence of paddles were solved separately for the moving frame; whilst at the interface, the two solutions obtained from both rotating and stationary frame of reference were matched locally via appropriate velocity transformations from one frame to another (Luo *et al.* 1994).

Governing equations

Under steady-state condition, the conservation of mass and momentum equation for a rotating frame of reference is given by Equations (source: Luo *et al.* 1994),

Continuity equation:

$$\frac{\partial \rho u_i}{\partial x_i} = 0 \tag{1}$$

Momentum equation:

$$\frac{\partial \rho u_j u_i}{\partial x_j} = -\frac{\partial p}{\partial x_i} + \frac{\partial \tau_{ij}}{\partial x_j} - 2\rho\varepsilon_{ijk}\Omega_j u_k + \rho\Omega_j(\Omega_j x_i - \Omega_i x_j) \tag{2}$$

The term $(2\rho\varepsilon_{ijk}\Omega_j u_k)$ in Equation (2) is the Coriolis acceleration and the term $\rho\Omega_j(\Omega_j x_i - \Omega_i x_j)$ represents the Centrifugal force acting on the fluid due to frame rotation. The stress tensor (τ_{ij}) is given by the standard $k-\varepsilon$ model as given in Equation (3),

$$\tau_{ij} = (\mu + \mu_t)\left[\left(\frac{\partial u_i}{\partial x_j} + \frac{\partial u_j}{\partial x_j}\right) - \left(\frac{2\partial u_k}{3\partial x_k}\delta_{ij}\right)\right] \tag{3}$$

The turbulent viscosity (μ_t) is calculated using the turbulent kinetic energy (k) and the dissipation rate (ε), given as $\mu_t = C_\mu \rho k^2/\varepsilon$.

Tracer studies modelling technique

The addition of tracer at the inlets of the middle floc tank was executed after the steady-state solution of the flow-field variables (velocity, turbulent kinetic energy, and turbulent dissipation energy) was acquired. The strategy was to include a scalar transport equation for a conservative species of known mass fraction and solve numerically in an unsteady mode for a certain period of time (Ta 1999; Choi *et al.* 2004; Baawain *et al.* 2006; Zhang 2006; Stamou 2008). Accordingly, tracer mass fraction of 1.0 was introduced at the inlet at time $(t) = 0$; possessing similar fluid property (density and viscosity) as that of water and with a mass diffusivity co-efficient of $1 \times 10^{-10}\,\mathrm{m^2\,s^{-1}}$. The corresponding mass fraction of tracer at each individual outlet port was monitored for every 15 s time interval for a total period of 2 h, using time steps of 35 s for convergence. A higher order quadratic upstream interpolation for convective kinetics (QUICK) scheme was used to solve the scalar transport Equation (4). QUICK finite difference scheme uses quadratic interpolation to estimate the tracer concentration value, on a space staggered grid, at the same location as the velocity components (Falconer & Ismail 1997). This scheme has shown to yield high accuracy in comparison with the more conventional second-order central difference representation and has been increasingly used in solving the advection-diffusion equations, particularly for modelling of tracer transport in chlorine contact tanks (Falconer & Liu 1988; Chen & Falconer 1992; Falconer & Ismail 1997; Wang & Falconer 1998) (source: Stamou 2008),

$$\frac{\partial \rho C}{\partial t} + \frac{\partial \rho u_j C}{\partial x_j} = \frac{\partial}{\partial x_i}\left(\rho\frac{\partial C}{\partial x_j} - \rho\overline{u_j C}\right) \tag{4}$$

The term $-\rho\overline{u_j C}$ is the turbulent mass flues, calculated as

$$-\rho\overline{u_j C} = \frac{\mu_t}{\sigma_C}\cdot\frac{\partial C}{\partial x_j} \tag{5}$$

Velocity gradient (G) and its calculation

The average velocity gradient (G) developed by Camp & Stein (1943) remains as the standard design parameter used by engineers to characterize the mixing process in flocculation basin (Crittenden *et al.* 2005; Bridgeman *et al.* 2008). However, the physical interpretation of G-values is not a velocity gradient, but rather the root mean energy dissipation per unit volume (Haarhoff & Van der Walt 2001) and is as described in Equation (6),

$$G = \sqrt{\frac{P}{\mu V}} = \sqrt{\frac{\varepsilon}{\nu}} \tag{6}$$

Accordingly, to calculate the desired G-value for the flocculation tank, the only variable required was the input power supplied for mixing. Input power requirements were calculated by using both traditional empirical and numerical modelling approaches. The power input for mixing is determined depending on the type of mixing device used and the empirical equation for horizontal paddles with three paddle boards (per arm) is estimated from Equation (7) (source: Crittenden *et al.* 2005).

$$P = \frac{1}{2}\rho C_D A_P\left[\frac{2\pi N(0.75)}{60\,\mathrm{s/min}}\right]^3\left(r_1^3 + r_2^3 + r_3^3\right) \tag{7}$$

The term $\left\{\left[\frac{2\pi N(0.75)}{60\,\mathrm{s/min}}\right]\cdot r\right\}$ represents the velocity of paddles; where, 0.75 = relative velocity of paddle with respect to the fluid; C_D the drag coefficient of the paddle (for turbulent regime) is related to the Re (Rouse 1946),

is given by Equation (8) as,

$$C_D = \frac{1}{Re^2} \cdot \frac{8}{\pi} \cdot \frac{F_D}{\rho v^2} \quad (8)$$

Normally, for flat paddle structure designs, approximate values of C_D at $Re > 10^3$ is obtained using length to width ratio and is treated as a constant (Rouse 1946; Crittenden *et al.* 2005).

For numerical approach, the turbulent dissipation rate for the flocculation tank at different mixing speeds was acquired using the standard $k-\varepsilon$ model. Using this, the overall power consumption was calculated by numerically integrating the local power consumption over the entire vessel contents (Bridgeman *et al.* 2008), expressed as in Equation (9),

$$P = \rho \int \epsilon \, dV \quad (9)$$

Mesh generation and boundary conditions

All the computations were performed under steady-state condition, treating fluid to be incompressible, and water as the only fluid phase in the tank with density of 998.23 kg m^{-3} and viscosity of 0.001002 kg m^{-1} s^{-1}. It was considered beneficial in terms of computational demand to model a single chamber for different rotational speeds at first; rather considering all the three floc tanks. Thus, the middle floc tank with identical inlet and outlet configuration results are only presented in this study. Fine tetrahedral cells (mesh) of 131,155 were generated for the moving zone whilst coarser tetrahedral cells (mesh) of 88,901 cells were formed for the stationary domain. The moving zone of the fluid (water) was set to a rotational speed of 1, 2, 5, 10, 15 and 20 rpm in counter clockwise direction, for each simulation while the stationary zone was kept fixed. The surface of paddles and shaft of the flocculator in the moving zone were assigned moving wall (i.e. the paddles and shaft boundary) with no slip boundary conditions and the rotational speed was set to 0 rpm with respect to the rotating coordinate (Versteeg & Malalasekara 1995; Vakili & Esfahany 2009). Through sensitivity analysis the total number of grids was fixed ranging from 330,594 to 511,654 cells, corresponding to the speed of rotation. A calculated total mass flow rate of 0.25 kg s^{-1} was assigned to the inlet ports. Whereas, each outlet port was specified separate pressure outlet boundary condition with the gauge pressure set to 0 atm. Both inlet and outlet turbulence intensities were set to 5%. The walls were specified standard wall function with no slip boundary condition and the interface was assigned interior boundary condition.

The discretization schemes (algorithm) used to solve the governing Equations (1–3) was SIMPLE for pressure-velocity coupling, STANDARD for pressure, second order upwind schemes for momentum, turbulent kinetic energy and turbulent dissipation energy. Convergence of solution was distinct when (a) the monitoring residuals of continuity equation was below the tolerance limit of 1×10^{-05} and the momentum equation along x, y and z directions were below 0.001, (b) the total mass flow rate imbalance between inlet and outlet was lesser than 0.2%, and (c) the velocity profile of the outlet surface remained constant with the increment in the number of iterations. All the computations were converged within ~2,000 iterations.

Experimental tracer studies

Experimental trails were performed through winter conditions, during which the average pH, alkalinity and temperature of the raw water in pilot-scale were 5.24, ~0 mg/L of $CaCO_3$ (below detection limit) and 13.8°C respectively. The characteristics of low pH and low alkalinity enabled the addition of alkali Sodium hydroxide (NaOH) chemical as the best available tracer option for evaluating the RTD of the pilot flocculation trains (Ives & Hoyer 1998). The sharp change in pH due to the addition of NaOH were electronically recorded using calibrated digital differential pH sensor (HACH company), placed near the outlet of the floc tanks, as shown in Figure 1. A solution of NaOH (1.0 M) was gradually pumped into the third rapid mix tank for achieving uniform flow condition of the tracer entering the inlet of the first floc tank. The increase in pH readings were continuously monitored until a steady-state value of pH (between 10 and 11) was attained at the outlets for all the three floc tanks. At this point of stability, the pump was shut down and the decrease in pH due to mixing and dilution of tracer with water was recorded for every 15 s time interval continuously for 2 h.

RESULTS AND DISCUSSIONS

Determination of RTD using experimental analysis

Time series plots for the decline in pH data were obtained. Readings recorded below pH of 5.5 were not taken into account due to the interference of natural background pH value of the raw water. In tracer analysis experiments, Ives & Hoyer (1998) explained that a change in pH of 1-unit reduces the hydroxyl ion concentration to $1/10^1$ or 0.1; thus 0.9 of the tracer has flowed out of the tank. Similarly, a change in pH of 2-units reduces the concentration to $1/10^2$ or 0.01 and again 0.99 of the tracer has left the tank and so forth. Based on this rationale, the displacement curves were acquired which represents the probability of tracer mass fraction exiting the tank outlet at theoretical HRT; helping in characterizing the flow as short circuiting and/or dead zones. Short circuiting is indicated by a time shift of curve to the left of theoretical HRT and the long tail or shift to the right of theoretical HRT indicates stagnation region (Ives & Hoyer 1998; Ta 1999).

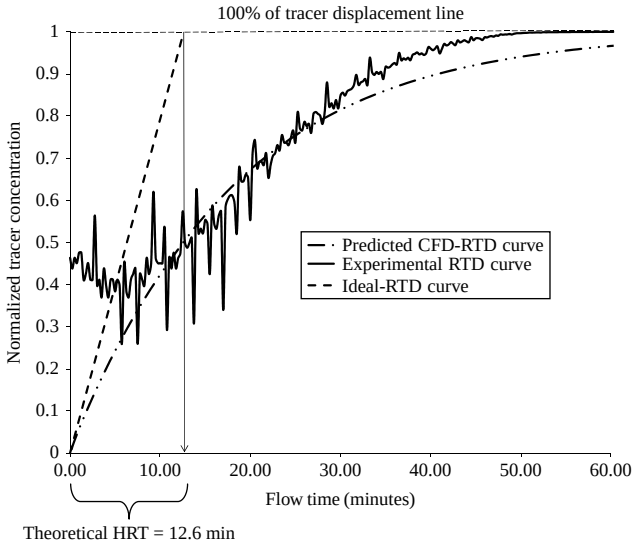

Figure 2 | Comparison of ideal, experimental and predicted CFD-RTD curve obtained using tracer studies conducted at a rotational speed of 14.3 rpm.

Comparison of experimental and CFD tracer analysis

Figure 2 compares the normalized mass fraction of the tracer displaced obtained using CFD and experimental tracer testing. Both the analyses were performed for 2 h time period at identical operating conditions (rotational speed of 14.3 rpm and temperature was 2°C). The middle-top outlet port (Figure 1) was considered to be more appropriate sampling location to monitor the predicted tracer concentration with that of experimental alkali analysis. The ideal RTD curve representing the maximum (100%) tracer displaced at theoretical HRT (12.6 min) was taken as reference for characterization of flow pattern. From Figure 2, both experimental and CFD curves have shifted afar to the right of the ideal curve. This indicates that substantial amount of tracer has been retained in the tank (for greater than theoretical HRT) largely due to prevalent mixing condition. Due to fluctuation in the initial pH readings, the displacement curve for the experimental results have not commenced ideally as that of CFD predictions; instead has started from 0.46 at $t = 0$ min. Figure 2 shows a reasonable agreement between the normalized mass fraction of the CFD and experimental tracer data. Approximately 50% of the simulated (CFD) tracer mass fraction exited the outlet while 57% for the experimental runs at theoretical HRT.

Drawbacks of experimental tracer studies

Tracer studies were economical and straightforward to perform at pilot-scale; however, the reproducibility of tracer trails was challenging as the pH probe had to be inserted manually near the top outlet (not a fixed sampling location). Successive alkali tracer studies for summer condition were not possible due to the commencement of coagulation studies, which would have otherwise interfered with the optimal pH required for alum dosing. Switching of the tracer option to other conservative chemical such as Fluoride seemed to be another reliable option. But the samples tested for Fluoride using HACH DR/4000U spectrophotometer using SPADNS method (APHA *et al.* 1998) showed inconsistent results. It was later found using the simulation (modelling) results of velocity contour profile that the location of sampling ports (Figure 1) were at potential dead zone; with no or minimum tracer existence in that area. Thus, CFD modelling could provide information about the existence and location of dead zones which would not be otherwise known (Templeton *et al.* 2006).

CFD simulation results

Analysis of influence of mixing speeds on the flow-field data

Figure 3(a, b) shows the effect of low (2 rpm) and high (20 rpm) rotational speeds on velocity contour profile along the radial plane at a mid-depth of 0.380 m respectively. In general, the water entering the tank experienced a drift from the axial (horizontal) direction at 2 rpm. In particular, the change in its direction was more prevalent through the middle inlet ports located at 0.035 m distance away from the outermost paddle board. It was evident from Figure 3(a) that the velocity of water flowing nearer the paddle arm region was higher than rest of the portion. In these low flow regions velocities were calculated to be as low as 0 to 0.025 m s^{-1}, indicating potential dead zones in the flocculation tank. In contrast, the existence of strong circulation patterns covering most of the tank volume was observed in Figure 3(b).

To analyze the effect of paddle mixing along the depth of the tank (i.e. along y coordinate), axial velocity vector were plotted at a distance of $x = 0.025$ m and width of $z = 0.272$ m for 2 and 20 rpm rotational speeds. Similar to the observations made by others (e.g. Luo 1997;

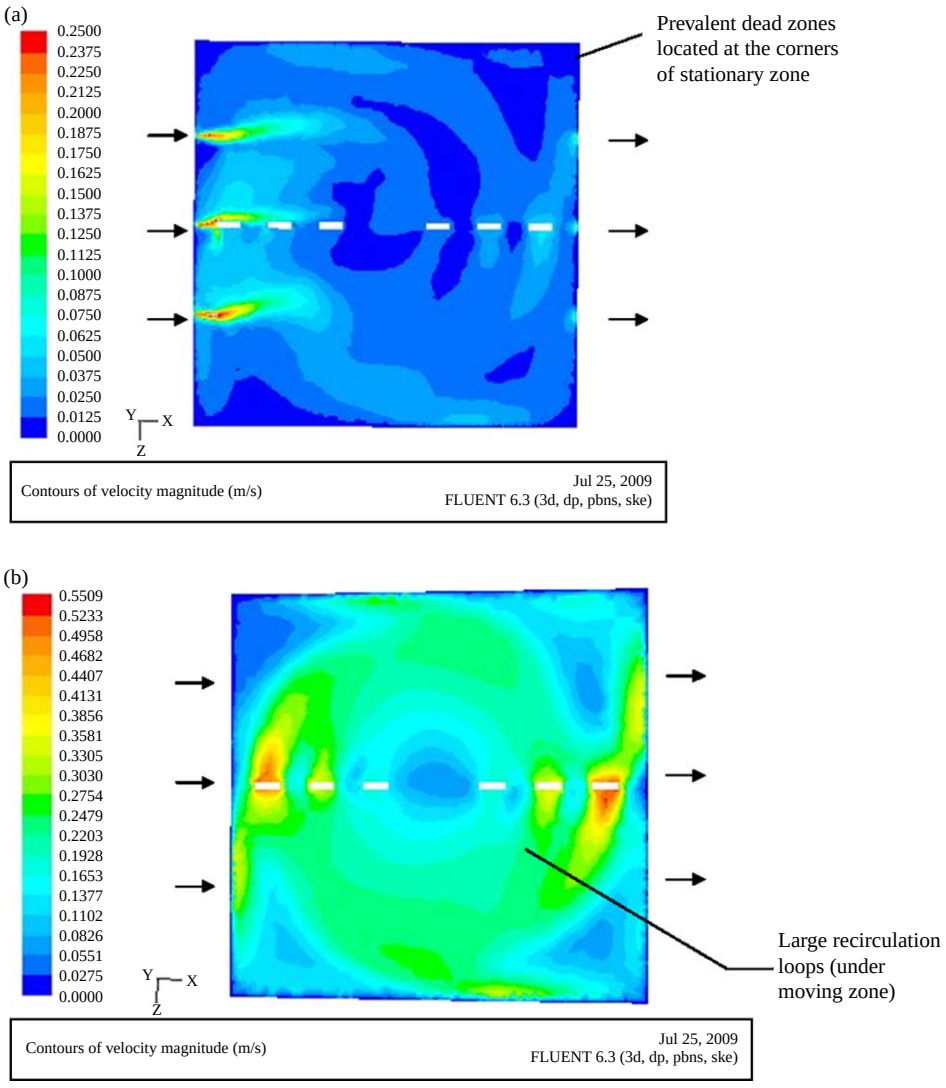

Figure 3 | Influence of rotational speeds on the contour profile of velocity magnitude along the radial plane at a mid-depth of 0.380 m of flocculation tank (a) 2 rpm (b) 20 rpm.

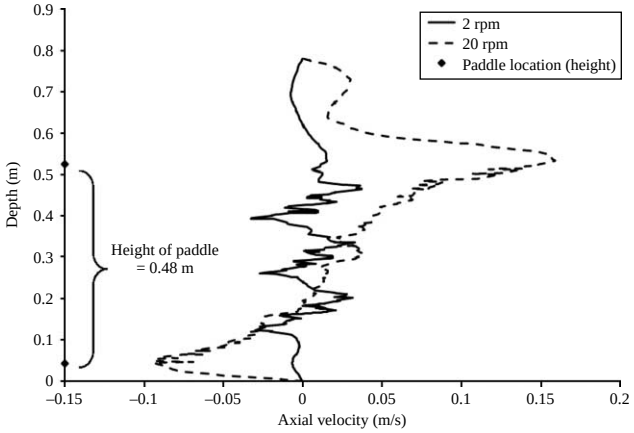

Figure 4 | Influence of rotational speeds on the axial velocity vector profile along the depth of the flocculation tank for 2 rpm and 20 rpm.

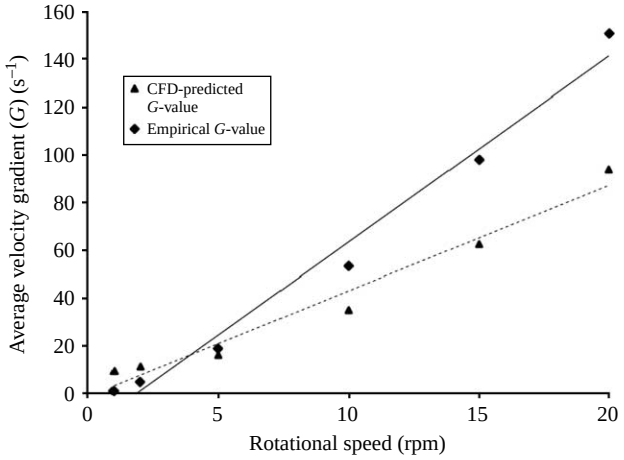

Figure 5 | Comparison of CFD-predicted and empirical *G*-values for different rotational speeds for the flocculation tank.

Shekhar & Jayanti 2002; Choi *et al.* 2004; Bridgeman *et al.* 2008), this study identified a radially outward pattern of water, which deflects by the tank wall and re-enters back into the moving zone. This phenomenon is more clearly observed at an operating speed of 20 rpm, as shown in Figure 4. The axial velocity vectors are highest above and below the paddle height at a depth of 0.044 and 0.525 m, taking positive and negative signs respectively. The interpretation of a positive or negative sign shown in Figure 4 relates to the vessel wall deflecting the fluid in the upward and downward direction above and below the impeller respectively (Bridgeman *et al.* 2008). At a rotational speed of 2 rpm, this characteristic pattern is diminished due to the influence of inlet ports located at 0.1685, 0.3005 and 0.4325 m along the depth. At this lower rotational speed, three sharp peaks having a negative axial velocity vector were observed.

Velocity gradient (*G*) value calculation for different mixing speeds

With the simulation results predicted for various rotational speeds, it can be therefore considered that there is predominant influence of paddles on mixing pattern at rotational speeds greater than 5 rpm. As represented by the large recirculation loops in the contours of velocity magnitude (Figure 3(b)). In order to find out the effect of mixing speed on flocculation process, the *G*-values were evaluated using both empirical and CFD approaches. As examined by Cornwell & Bishop (1983), Figure 5 shows a linear relation between the *G* and *N* values for both empirical and numerical predictions. The empirical *G*-values calculated for 1 and 2 rpm using Equations (6) and (7) were lower than CFD predictions, as observed from Figure 5. However, there is significant agreement between them up to 5 rpm. With further increase in the rotational speed, the magnitude of *G*-values is considerably increased using empirical method. For highest rotational speed of 20 rpm, the empirical *G*-value was about 151 s^{-1} while it was found to be 94 $s^{-1}$from CFD analyses.

To analyze the reason behind the discrepancy, the variables used for the calculation of *G*-value in Equations (6–9) were examined. It was evident from Equation (8) that the constant drag coefficient value of 1.38 negated the impact of changing rotational speeds and *Re*. Thus, a sensitivity analysis was conducted by varying the drag coefficient values to 1.90, 1.50, 1.16, 1.0 and 0.7; based on the C_D values provided for different paddle length to width ratios (Rouse 1946; Crittenden *et al.* 2005). Figure 6 shows that for a C_D of 0.7, the *G*-values calculated by empirical equations for rotational speeds greater than 5 rpm was substantially reduced and was nearly equal to that of the predicted *G*-values. For C_D values greater than 1.38, the deviation from predicted *G*-value was steadily increasing. Thus, with the help of sensitivity analysis the C_D value of 0.7 was considered optimal for minimizing the variation caused at $Re > 20{,}000$.

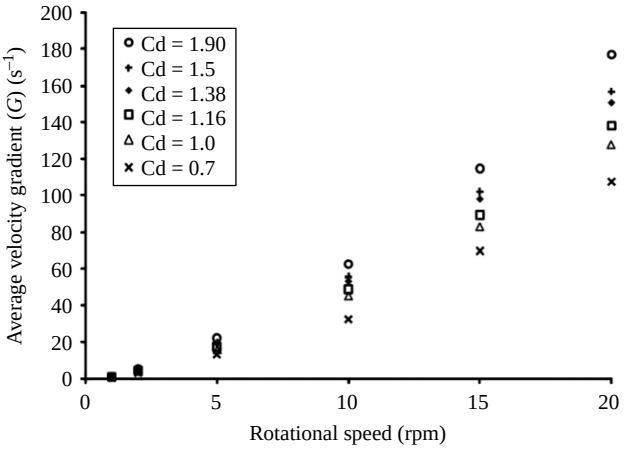

Figure 6 | Sensitivity analysis for investigating the effect of drag coefficient values on the empirical *G*-value calculated.

The *G*-values thus obtained by tuning the C_D to 0.7 were plotted against the CFD predictions, as shown in Figure 7. Even though, there is reasonable agreement between the two techniques; there is contrary impact on the *G*-values calculated at 1 and 2 rpm. At these operational speeds, the magnitude of empirical *G* has dropped considerably to 0.69 and 3.4 s^{-1} respectively; stating that there is lower rate of dissipation of energy throughout the tank volume. On the other hand, *G*-values of CFD prediction were 9.1 and 11 s^{-1} for 1 and 2 rpm respectively, obtained using the local dissipation rate. This significant difference exemplifies the flexibility and precision of using CFD for different flow conditions in terms of energy input required for suspension

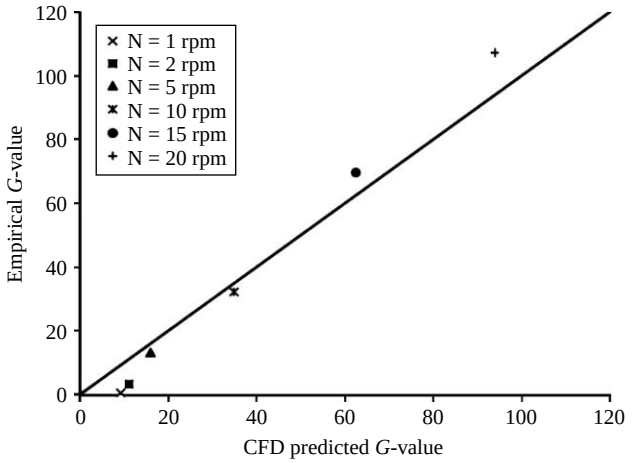

Figure 7 | Plot of CFD-predicted and empirical *G*-values calculated at $C_D = 0.7$ for different rotational speeds for the flocculation tank (line of equivalence is shown at 45° for reference purposes).

of flocs formed. Nevertheless more rigorous experimental analysis are needed for calculating the drag coefficient for different rotational speeds and consequently, arriving at the desired *G*-values.

CONCLUSIONS

The results presented in this study shows that CFD can be considered as a valuable technique to capture the complex turbulent flow characteristics of paddle flocculators of pilot-scale systems. It was observed from the flow-field analysis that uniform mixing pattern was achieved extending throughout the tank volume at relatively lower rotational speeds due to the unique paddle board configuration. Almost 62% of the overall depth of the tank is occupied by the three pairs of paddle, which brings about uniform mixing and suspension of water for rotational speeds greater than 5 rpm. Thus, the average *G*-values typically used for tapered paddle flocculation process (up to 60 s^{-1}) can be achieved at lower rotational speed (around 15 rpm); minimizing the power input required for mixing. In contrast, the *G*-values of empirical method are substantially higher than the predicted values for rotational speeds greater than 5 rpm and showed decreased energy rates at 1 and 2 rpm. Further sensitivity analysis of the drag coefficient C_D used in empirical method, showed that thorough experimental analysis are required to optimize the C_D for various rotational speeds. The practical implications of operating at higher than required *G*-values relates to potential negative consequences such as floc break up, the reliance of chemical additives to avoid floc break-up and the increased carbon footprint through higher energy demands.

It was possible to obtain the actual local turbulent dissipation rate directly through CFD simulation. In comparison to the difficulty of obtaining precise in situ field measurements, the CFD simulations provided an accurate, economical method for determining the conventional design parameter (*G*-value) for the given pilot-scale design. Thorough evaluation of the hydrodynamics of flow will help in establishing proper design parameter for a given flocculation unit and subsequently provides a novel strategy for improved management of chemical and optimization of the overall water quality outcomes.

ACKNOWLEDGEMENTS

The authors would like to acknowledge and thank Halifax Water and Natural Sciences and Engineering Resource Council of Canada (NSERC) for financial support to the NSERC/Halifax Water Industrial Research Chair. The authors also acknowledge the support provided by the plant staff at JDKWSP, Heather Daurie (Research Technician, Dalhousie University), Jessica MacKay (Research Technician, Dalhousie University) and Alisha Knowles (PhD Student, Dalhousie University) during pilot-scale tracer studies. Lastly, the authors appreciated the technical assistance provided by Krishna Podila (PhD Candidate, Dalhousie University) in model calibration.

REFERENCES

Argaman, Y. A. 1971 Pilot-plant studies of flocculation. *J. Am. Water Works. Assoc.* **63**(12), 775–777.

Baawain, M. S., Gamal El-Din, M. & Smith, D. W. 2006 Computational fluid dynamics application in modeling and improving the performance of a storage reservoir used as a contact chamber for microorganism inactivation. *J. Environ. Eng. Sci.* **5**(2), 151–162.

Baek, H., Park, N., Kim, J., Lee, S. & Shin, H. 2005 Examination of three-dimensional flow characteristics in the distribution channel to the flocculation basin using computational fluid dynamics simulation. *J. Water Supply Res. Technol.–AQUA* **54**(6), 349–354.

Betancourt, W. Q. & Rose, J. B. 2004 Review: drinking water treatment process for removal of *Cryptosporidium* and *Giardia*. *Vet. Parasitol.* **126**(1–2), 219–234.

Black, A. P., Buswell, A. M., Eidsness, F. A. & Black, A. L. 1957 Review of the jar test. *J. Am. Water Works Assoc.* **49**(11), 1414–1424.

Bridgeman, J., Jefferson, B. & Parsons, S. 2008 Assessing floc strength using CFD to improve organics removal. *Chem. Eng. Res. Des.* **86**(8), 941–950.

Camp, T. R. & Stein, P. C. 1943 Velocity gradients and internal work in fluid motion. *J. Boston Soc. Civ. Eng.* **30**, 219–237.

Chen, Y. P. & Falconer, R. A. 1992 Advection diffusion modeling using the modified QUICK scheme. *Int. J. Numer. Methods Fluids* **15**(10), 1171–1196.

Choi, B. S., Wan, B., Philyaw, S., Dhanasekharan, K. & Ring, T. A. 2004 Residence time distributions in a stirred tank: comparison of CFD predictions with experiment. *Ind. Eng. Chem. Res.* **43**(20), 6548–6556.

Craig, K., de Traversay, C., Bowen, B., Essemiani, K., Levecq, C. & Naylor, R. 2002 Hydraulic study and optimisation of water treatment processes using numerical simulation. *Water Sci. Technol. Water Supply* **2**(5–6), 135–142.

Crittenden, J. C., Trussell, R. R., Hand, D. W., Howe, K. J. & Tchobanoglous, G. 2005 *Water Treatment Principles and Design*, 2nd edition. John Wiley & Sons, Inc, Hoboken, New Jersey.

Cornwell, D. A. & Bishop, M. M. 1983 Determining velocity gradients in laboratory and full-scale systems. *J. Am. Water Works Assoc.* **75**(9), 470–475.

Downey, D., Giles, D. K. & Delwiche, M. J. 1998 Finite element analysis of particle and liquid flow through an ultraviolet reactor. *Comput. Electron. Agric.* **21**(2), 81–105.

Ducoste, J. J. & Clark, M. M. 1999 Turbulence in flocculators: comparison of measurements and CFD simulations. *AlChE J.* **45**(2), 432–436.

Dugan, N. R., Fox, K. R., Owens, J. H. & Miltner, R. J. 2001 controlling *Cryptosporidium* oocysts using conventional treatment. *J. Am. Water Works Assoc.* **93**(12), 64–76.

Essemiani, K. & de Traversay, C. 2002 Optimisation of flocculation process using computational fluid dynamics. *Proceedings of the 10th Gothenburg Symposium on Chemical Water And Wastewater Treatment VII*, 17–19 June, Gothenburg, Sweden.

Falconer, R. A. & Ismail, A. I. B. M. 1997 Numerical modeling of tracer transport in a contact tank. *Environ. Int.* **23**(6), 763–773.

Falconer, R. A. & Liu, S. 1988 Modeling solute transport using QUICK scheme. *J. Environ. Eng. ASCE* **114**(1), 3–20.

Gao, B. Y., Hahn, H. H. & Hoffmann, E. 2002 Evaluation of aluminum-silicate polymer composite as a coagulant for water treatment. *Water Res.* **36**(14), 3573–3581.

Haarhoff, J. & Van der Walt, J. J. 2001 Towards optimal design parameters for around-the-end hydraulic flocculators. *J. Water Supply Res. Technol.–AQUA* **50**(3), 149–159.

Ives, K. J. & Hoyer, O. 1998 Tracer studies of the hydraulics of tapered flocculation. *Water Sci. Technol.* **37**(10), 69–77.

Lerch, A. 2008 *Fouling layer formation by flocs in inside-out driven capillary ultrafiltraion membranes*. PhD thesis, University of Duisburg-Essen, Germany.

Luo, C. 1997 *Distribution of velocities and velocity gradients in mixing and flocculation vessels: comparison between LDV data and CFD Predictions*. PhD thesis, New Jersey Institute of Technology, New Jersey, USA.

Luo, J. Y., Issa, R. I. & Gosman, A. D. 1994 Prediction of impeller induced flows in mixing vessels using multiple frames of reference. *Inst. Chem. Eng. Symp. Ser.* **136**, 549–556.

Marcos, B., Moresoli, C., Skorepova, J. & Vaughan, B. 2009 CFD modeling of a transient hollow fiber ultrafiltration system for protein concentration. *J. Membr. Sci.* **337**(1–2), 136–144.

Nieminski, E. C. & Ongerth, J. E. 1995 Removal of *Giardia* and *Cryptosporidium* by conventional treatment and direct filtration. *J. Am. Water Works Assoc.* **87**(9), 96–106.

Rouse, H. 1946 *Elementary Mechanics of Fluids*. John Wiley & Sons, Inc, New York, USA.

Shekhar, S. M. & Jayanti, S. 2002 CFD study of power and mixing time for paddle mixing in unbaffled vessels. *Chem. Eng. Res. Des.* **80**(A5), 482–498.

Stamou, A. I. 2008 Improving the hydraulic efficiency of water process tanks using CFD models. *Chem. Eng. Process.* **47**(8), 1179–1189.

Standard Methods for the Examination of Water and Wastewater 1998 20th edition. American Public Health Association/ American Water Works Association/Water Environment Federation, Washington, DC.

States, S., Tomko, R., Scheuring, M. & Casson, L. 2002 Enhanced coagulation and removal of *Cryptosporidium*. *J. Am. Water Works Assoc.* **84**(11), 67–77.

Subramani, A., Kim, S. & Hoek, E. M. V. 2006 Pressure, flow, and concentration profiles in open and spacer-filled membrane channels. *J. Membr. Sci.* **277**(1–2), 7–17.

Svrcek, C., Guest, R. K. & Smith, D. W. 2006 Residence time distribution analysis of an intermittently operating truck fill facility to determine effective contact time. *J. Environ. Eng. Sci.* **5**(S1), S53–S67.

Ta, T. C. 1999 Current CFD tool for water and waste water treatment processes. *PVP- Emerg. Technol. Fluids Struct. Fluid/Struct. Interact.-ASME* **396**, 79–85.

TeKippe, R. J. & Ham, R. K. 1970 Coagulation testing: a comparison of techniques.1. *J. Am. Water Works Assoc.* **62**(9), 594–602.

Templeton, M. R., Hofmann, R. & Andrews, R. C. 2006 Case study comparisons of computational fluid dynamics (CFD) modeling versus tracer testing for determining clearwell residence times in drinking water treatment. *J. Environ. Eng. Sci.* **5**(6), 529–536.

Vakili, M. H. & Esfahany, M. N. 2009 CFD analysis of turbulence in a baffled stirred tank, a three-compartment model. *Chem. Eng. Sci.* **64**(2), 351–362.

Versteeg, H. K. & Malalasekera, W. 1995 *An Introduction to Computational Fluid Dynamics: The Finite Volume Method*, 1st edition. Pearson Education Limited, Harlow, England.

Wang, H. & Falconer, R. A. 1998 Simulating disinfection process in chlorine contact tanks using various turbulence models and high-order accurate difference schemes. *Water Res.* **32**(5), 1529–1543.

Wols, B. A., Uijttewaal, W. S. J., Rietveld, L. C., Stelling, G. S. & Dijk, J. C. 2008 Residence time distributions in ozone contactors. *Ozone. Sci. Eng.* **30**(1), 49–57.

Xagoraraki, I., Harrington, G. W., Assavasilavasukul, P. & Standridge, J. H. 2004 Removal of emerging waterborne pathogens and pathogen indicators. *J. Am. Water Works Assoc.* **96**(5), 102–113.

Zhang, J. 2006 *An integrated design approach for improving drinking water ozone disinfection treatment based on computational fluid dynamics*. PhD thesis, University of Waterloo, Canada.

Zhang, J., Huck, P. M., Stubley, G. D. & Anderson, W. B. 2008 Application of a multiphase CFD modelling approach to improve ozone residual monitoring and tracer testing strategies for full-scale drinking water ozone disinfection processes. *J. Water Supply Res. Technol.–AQUA* **57**(2), 79–92.

First received 26 August 2009; accepted in revised form 22 March 2010